NIH Public Access
Author Manuscript
J Magn Reson. Author manuscript; available in PMC 2014 September 20.

Published in final edited form as:
J Magn Reson. 2013 April ; 229: 67–74. doi:10.1016/j.jmr.2012.11.012.

Engineering Novel Detectors and Sensors for MRI

Chunqi Qian[¶,1], **Gary Zabow**[¶,1,2], and **Alan Koretsky**[*,1]

[1] National Institute of Neurological Disorders and Stroke, National Institutes of Health, Bethesda, MD, 20892

[2] Electromagnetics Division, National Institute of Standards and Technology, Boulder, CO, 80305

Abstract

Increasing detection sensitivity and image contrast have always been major topics of research in MRI. In this perspective, we summarize two engineering approaches to make detectors and sensors that have potential to extend the capability of MRI. The first approach is to integrate miniaturized detectors with a wireless powered parametric amplifier to enhance the detection sensitivity of remotely coupled detectors. The second approach is to microfabricate contrast agents with encoded multispectral frequency shifts, whose properties can be specified and fine-tuned by geometry. These two complementary approaches will benefit from the rapid development in nanotechnology and microfabrication which should enable new opportunities for MRI.

Keywords

Micro resonator; inductive coupling; Microfabrication; contrast agents

Introduction

Small is beautiful. An old adage, but one that seems ever more prescient in today's age of miniaturization. Scaling down need not just be about squeezing more transistors onto a silicon chip; often it is about creating new tools to develop improved capabilities. The burgeoning field of nanobiotechnology is replete with many examples of novel materials some of which have impacted MRI, such as small iron oxide particles. It is clear the full potential of modern microfabrication technique is just beginning to be realized. Microresonator for MRI is an obvious example when miniaturization offers advantages. Microcoils are not just scaled down versions of their macroscopic counterparts; they offer demonstrably greater mass sensitivities [1, 2] and, if sufficiently small, can be advantageously employed in-vivo [3–15], further enhancing SNR compared to external surface coils [16, 17], or providing unique image contrast [18]. Going beyond detectors,

[*] *Correspondence*: Alan P. Koretsky 10 Center Dr. Room 1D728, MSC 1065 Bethesda, MD, 20892-1065 Tel.: +1 (301) 402-9659; Fax: +1 (301) 480-2558 koretskya@ninds.nih.gov.
[¶] These authors contribute equally to this work.

Publisher's Disclaimer: This is a PDF file of an unedited manuscript that has been accepted for publication. As a service to our customers we are providing this early version of the manuscript. The manuscript will undergo copyediting, typesetting, and review of the resulting proof before it is published in its final citable form. Please note that during the production process errors may be discovered which could affect the content, and all legal disclaimers that apply to the journal pertain.

NIH-PA Author Manuscript
NIH-PA Author Manuscript
NIH-PA Author Manuscript

NIH-PA Author Manuscript

NIH-PA Author Manuscript

NIH-PA Author Manuscript

however, contemporary micro- and nanofabrication technologies now routinely yield functional structures two orders of magnitude smaller than the size of a typical biological cell. As micro and nanotechnology research fields grow, so too do the prospects for various new forms of engineered in-vivo MRI micro- and nanoprobes that could allow imaging and sensing in locations, and at local size scales, unachievable previously.

In this brief perspective, we consider two recent examples of our ongoing work into new engineered detectors and sensors with potential for *in-vivo* applications. The first is a wireless microcoil resonator that exploits parametric amplification to overcome inductive coupling losses and enhance in-vivo MRI sensitivity. This coil has promise for miniaturization. The second concerns magnetic micro- and nanostructures that are engineered to controllably shift the resonances of neighboring MRI-detectable nuclei, providing new MR imaging and sensing opportunities.

Wireless Amplified NMR Detector (WAND) for MRI

It is well known in the magnetic resonance community that a smaller coil has higher detection sensitivity when it is placed in the vicinity of the detection object [19]. But traditionally, when local coils are used as implanted or interventional detectors inside the body, the detected signal needs to be transmitted out either through direct cable connections or wireless inductive coupling. The direct cable connection has been used extensively for catheter coils [20–22], but the associated heating induced by the RF excitation can be problematic [23–25]. Metamaterials [26–28] and optical fibers [29–31] have been recently proposed as alternative signal transmission media to improve RF safety. However, the requirement for wired connections makes the local detection coil clumsy for a number of applications, such as a chronic implantable device.

Wireless inductive coupling [32] has been used to eliminate wires; however, the separation between the local detector and the external surface coil must be small if the sensitivity is to be maintained. It would be ideal if the internally detected signal can be amplified *in situ* before being transmitted wirelessly to the external surface coil, so that the superior sensitivity of the local detector can be taken advantage of with a remote detector. To achieve such a goal, a transistor-based low-noise amplifier is difficult to use, because it requires a DC power source that is difficult to provide wirelessly. On the other hand, parametric amplification has been recently used as an alternative scheme for MR signal amplification [33–36], but its common implementation with a reverse-biased varactor necessitates the use of a cable connection. Recently, we have demonstrated that a wireless parametric resonator can utilize externally provided power for signal amplification [37]. The design uses a zero-biased varactor circumventing bias connections enabling efficient frequency mixing with very low power consumption. Since the frequency response of the parametric resonator can be wirelessly adjusted by the external power source, it is possible to detune the resonator during transmit and retune the resonator during signal reception. Below is a brief summary of the basic properties of a wireless parametric amplifier, based on the theoretical analysis in references [37, 38].

NIH-PA Author Manuscript

NIH-PA Author Manuscript

NIH-PA Author Manuscript

Fig. 1a is the circuit diagram of a wireless parametric amplifier. The core component is a nonlinear triple frequency resonator with one capacitor C_2 substituted by a zero-biased varactor. The circuit is constructed such that the sum of the lower two resonance frequencies is approximately equal to the third one. If the input RF signal has a frequency ω_1 that is close enough to the lowest resonance frequency of the resonator, the weak input signal can mix with a strong pumping signal at ω_3 provided by the external pumping loop (Fig. 1b). Such a frequency mixing process can produce an amplified output at the idler frequency $\omega_2 = \omega_3 - \omega_1$, which can again mix with the pumping signal at ω_3 to produce a secondary output with gain at ω_1. As a result, the amplified signal can be detected by an external pickup loop at the input frequency ω_1 as well. For MR applications, the input frequency ω_1 is the same as the Larmor frequency, and the operating frequencies ω_1, ω_2, and ω_3 are normally not equal to the resonance frequencies ω_{10}, ω_{20} and ω_{30}, especially when the isolated resonator is embedded inside the body and detuned by its surrounding tissues. However, efficient amplification still occurs when the frequency matching condition is satisfied:

$$\frac{2\mathscr{Q}_1(\omega_1-\omega_{10})}{\omega_{10}}=\frac{2\mathscr{Q}_2(\omega_2-\omega_{20})}{\omega_{20}}\equiv\kappa \quad (1)$$

where Q_1 and Q_2 are quality factors at ω_{10} and ω_{20} respectively. The power gain for output signal at ω_1 can be estimated from the extent to which the resonator deviates from the oscillation condition:

$$G_{1\to1}\approx\frac{1}{4}\left(\frac{M_0}{M_0-M}\right)^2 \quad (2)$$

M is the modulation index defined in the capacitance modulation function $C_2(t)=C_2(1+2M\cos\omega_3 t)$, where C_2 is the varactor capacitance at zero bias, and M_0 is the modulation index required for circuit oscillation:

$$M_0=\sqrt{\frac{1+\kappa^2}{\mathscr{Q}_1\mathscr{Q}_2}} \quad (3)$$

This equation indicates that the threshold modulation index M_0 is required to “refresh” the dissipated energy in the circuit $\left(1/\sqrt{\mathscr{Q}_1\mathscr{Q}_2}\right)$. Such an energy compensation process leads to a decreased circuit resistance so that the effective bandwidth of a parametric resonator is inversely proportional to the square root of power gain $\sqrt{G_{1\to1}}$:

$$\frac{2\Delta\omega}{\omega_1}\sqrt{G_{1\to1}}\approx\frac{1}{\mathscr{Q}_1+(\omega_1/\omega_2)\mathscr{Q}_2} \quad (4)$$

Parametric amplification generates extra noise, because noise from both ω_1 and ω_2 are amplified while the MR signal to be amplified exists only at ω_1. When compared to a passive detector with a direct cable connection, the noise factor of a parametric resonator is:

NIH-PA Author Manuscript

NIH-PA Author Manuscript

NIH-PA Author Manuscript

$$F=\frac{G_{1\to1}+G_{2\to1}}{G_{1\to1}}=1+\frac{\omega_1}{\omega_2} \quad (5)$$

where $G_{2->1}$ is the conversion gain for noise originating from the ω_2 band. This conversion gain $G_{2->1}$ is related to the power gain $G_{1->1}$ by a scaling factor equal to the output-to-input frequency ratio ω_1/ω_2 according to the Manley-Rowe relation [39]. The detection sensitivity on the external surface coil can be estimated from the signal-to-noise power ratio:

$$\left(\frac{S}{N}\right)_1=\frac{S_0E_1G_{1\to1}}{N_1F_1E_1G_{1\to1}+N_{Lp1}} \quad (6)$$

where S_0 is the signal power generated by the nuclei spins, N_1 is the noise power originating from the local resonator, N_{Lp1} is the noise power originating from the pickup loop (loop 1), and E_1 is the transmission efficiency, that is, the power delivered to the pick up loop per unit power originating from the local resonator. If there is sufficient gain to yield $E_1G_1>>1$, the noise of the parametric resonator can dominate over the external surface coil, and the *SNR* is S_0/N_1F_1, which is comparable to that of a local resonator with a direct cable connection.

For simplified circuit construction, the triple frequency resonator can be reduced to a double frequency resonator (Fig. 1c) by making the idler and the Larmor frequency share a single circuit mode ($\omega_2 \approx \omega_1$). The resonator was constructed by simultaneously connecting a chip capacitor C_1 (5.1 pF, ATC100A) with two orthogonal inductors (L_1 and L_2). L_1 was a one-and-half turn solenoid wrapped around a rectangular rod with a side length of 1.5 mm. L_2 was a two-and-half turn solenoid wrapped around a 1.9 mm diameter cylindrical rod. To create a second resonance mode, L_2 was split in the center and reconnected by a zero-biased varactor (BBY52-02L, Infineon Technologies). The resonator was then immersed in a PDMS mixture and cured at 40 degree for 12 hours. In order to differentiate the amplified outputs at these two frequencies, it is necessary to separate ω_2 and ω_1 by a difference frequency that is larger than the receiver bandwidth of the MRI system. Such a “degenerate” mode of parametric amplification has a noise factor of 2, which is larger than that of a low-noise transistor based amplifier. However, the double resonant parametric resonator has a sensitivity advantage under weak coupling conditions, when the sensitivity loss due to parametric amplification can be negligible compared to the sensitivity gain due to local signal detection.

As a practical demonstration of such a sensitivity advantage in a preclinical animal model, a millimeter-scale wireless amplified detector was constructed using the scheme in Fig. 1c. This small detector could be chronically implanted onto the medial surface of a rat kidney. This is a deep lying region inside the body far from an external surface coil. For a penetration depth of 15 mm, which is much larger than the detector's own dimension, the parametric resonator is 12 dB more sensitive than a passive resonator and 21 dB more sensitive than the external surface coil. With such greatly improved sensitivity and proper choice of contrasts, it is possible to obtain high-resolution images of the kidney to identify renal tubules (Fig. 2c) and glomeruli (Fig. 2d) *in vivo*. For larger penetration depths and further miniaturization, the power gain may not be sufficient to preserve the local detector's *SNR*, but the parametric resonator remains much more sensitive than a passive resonator or

NIH-PA Author Manuscript

NIH-PA Author Manuscript

NIH-PA Author Manuscript

an external surface coil. The parametric resonator may be useful in intravascular or rectal applications where the wireless detector can be placed close to the object, for intestinal applications where the detector can be swallowed, and for bioengineered tissue constructs where the detector can be imbedded.

Microengineered Multi-spectral Contrast Agents for MRI

A second, quite different, example of an engineered structure for MRI can be found in recently demonstrated microengineered, multispectral contrast agents [40]. These micro- to nano-scale engineered magnetic structures are designed to controllably alter the resonance frequencies of water, or of any other MR-detectable nuclei, in their local vicinity. They may therefore be regarded as engineered resonance shifters, with most obvious application as new types of selectively addressable, frequency-dependent contrast agents.

At their core, is the idea of an engineered magnetic structure containing an open, water-accessible magnetic “cavity” in which the magnetic field profile is tailored to enable discrete frequency shifting of the NMR water line. This discrete frequency shifting is in contrast to the more usual linewidth broadening that accompanies the transverse dephasing caused by the dipolar-like fields surrounding all magnetic structures. Key to the functioning of these resonance shifting agents, which are after all magnetic structures themselves, is the fact that even though spatially decaying fields are unavoidable in the far-field regions of all magnetic particles, the same is not true in nearby field regions. In particular, for specially designed cavity-like geometries, in regions close to the particle, fields can be highly homogeneous over extended spatial volumes. This results in local Larmor precession frequencies that can be the same in the uniform field region within the cavity, but that are shifted away from the precession frequencies outside the cavity. With their uniform internal fields, these hollow microparticle structures each form a localized, miniature magnet within the external magnet, where the B_0 field within each microparticle cavity can be individually engineered to be different from the B_0 of the main magnetic field. In effect, each structure can therefore have a distinct NMR shift much like the distinct NMR chemical shift of different molecules. The difference with an artificially engineered structure is that its NMR shift is determined not by any local chemical structure, but instead by the microengineered geometry and material that allows direct tuning of the frequency shift.

Although spatially extended uniform fields require precisely defined surrounding magnetic particle dimensions, there are multiple different families of geometries that can all, to greater or lesser degree, produce the requisite locally uniform shifted field profiles. As some examples, in our work we have demonstrated such multispectral agents based on pairs of parallel, spaced disks [40, 41], based on short, hollow cylinders [42], and, most recently, based on ellipsoidally shaped material shells (in preparation). A schematic of such geometries, along with representative scanning electron micrographs (SEM) of actual microfabricated structures is shown in Fig. 3. Taking the double-disk structure as an example, Fig. 4 shows the theoretical magnetic field profile that would result in the cavity region between two appropriately spaced, parallel disks when they are magnetized to saturation by the MRI B_0 field. In this example, the B_0 field is assumed oriented parallel to the plane of the disks. Minimization of magnetic shape anisotropy energy for thin disks

NIH-PA Author Manuscript

NIH-PA Author Manuscript

NIH-PA Author Manuscript

implies that this is the natural preferred orientation of such structures when placed in an applied field. Also shown is a histogram of the field magnitudes, or equivalently, of the local precession frequency values, within and around the structure cavity, providing a first order approximation of the NMR spectrum from such a structure. The frequency-shifted offset peak, which for a double-disk geometry can have a linewidth as narrow as $1/100^{th}$ of the frequency shift magnitude itself, results from the uniform field region created between the disks. It is this frequency-shifted peak which serves as the distinguishing NMR spectral signature of the structure and can be shifted in frequency by changing any of disk radii, thicknesses, spacings, or materials.

While spectral linewidths depend on the degree of field uniformity, the amount by which the linewidth is shifted depends on the magnitude of the field generated within the particle cavity. Regardless of the particular family of geometries chosen, for all structures this field magnitude is independent of overall structure size, but does depend on structure aspect ratios and on the magnetic saturation polarization densities of the magnetic materials comprising the structure. Given the structure geometries and their required precision, it has thus far proven easier to microfabricate, rather than chemically synthesize, these agents. Although microfabrication often entails more lengthy and complex processing steps, its more physical, rather than chemical, nature means that changing these structure aspect ratios and materials is relatively straightforward. High-magnetic-moment and biocompatible materials can be readily combined and interchanged, coatings can be added that are either biologically inert, such as titanium, or specifically conducive to biofunctionalization, such as gold. Aspect ratios can be adjusted, allowing multiple different resonance shifts to be produced on demand for multiplexed, multispectral, or so-called “color”, MRI. In effect, although the physical operating principles may be quite different, the engineered multispectral agents can therefore be regarded as RF analogs of engineered optical quantum dots [44–46] or optically resonant plasmonic nanoparticles [47] that, together with other multicolor labels and dyes [48], have fueled much of the boom in cellular and molecular biological research.

There are other multispectral MRI contrast agents based on chemical exchange saturation transfer (CEST) protocols (and variants thereof) that have enjoyed considerable success [49–52]. In many ways these other agents are more accessible to researchers, because they are substantially easier to synthesize or are comprised of chemical compounds that are readily available. But a distinction between chemically based agents and microengineered material ones, is precisely the ability to directly “engineer”, or tailor, agent properties to finely tune resonances, enhance functionality, or to otherwise optimize performance for each particular intended application. With agent function being essentially independent of overall agent size, from macroscopic down to microscopic, such applications may be many and varied. If superparamagnetic, or ferromagnetic materials are used, resonances can be tuned over an unusually broad spectral range that can span tens of megahertz. Materials used are readily saturated by all conventional B_0 fields, so these large resonance shifts can be achieved even in low field MRI. Broad spectral shift ranges permit simultaneous use of, and discrimination between, many different resonance shifting agents. Large shifts also aid discrimination from background water signals. Due to the large shift, constraints on RF pulse shapes are considerably reduced. These agents are also distinguished from chemically based counterparts in that, being particulate based, they simultaneously function as both

NIH-PA Author Manuscript

NIH-PA Author Manuscript

NIH-PA Author Manuscript

multispectral, and as regular T_2* dephasing agents. While the discrete resonance shifting properties arise from the shape-dependent local fields, the surrounding T_2* dephasing properties are always also present, arising predominantly from more distant regions where the signal is independent of the particle shape. This dual functioning means, for example, that these agents can be used as tags for such applications as cell monitoring and tracking, much like that performed with traditional chemically synthesized iron-oxide particles [53] such as SPIOs [54, 55] or MPIOs [56]. A difference is that while their T_2* effects provide the same spatial localization as do MPIO's, their unique co-localized spectral signatures allow for distinguishing beween agents, and therefore, if specifically targeted, for simultaneous tracking of, and distinction between, multiple cell types. The spectral signatures also allow observed dephased signal regions to be unequivocally associated with the actual contrast agent, rather than with other incidental hypointense signals that might result from, say, an air bubble or some other endogenous local variation in magnetic susceptibility. Additionally, as discussed below, the agents' spectral signatures can potentially provide information on the local environment.

An example of this simultaneous T_2* and multispectral behavior is shown in Fig. 5 which shows gradient echo and chemical shift images obtained from sets of agents whose resonances were varied by changing the thickness of the magnetic disks comprising those agents. Also shown are the NMR spectra with the shifted resonance that the agents generate. From basic operational and biocompatibility viewpoints, it is interesting to note that this added multispectral agent functionality does not require any different materials from those in regular SPIO and MPIO agents. Ultimately, it is only the spatial redistribution of the material that is involved, remolding it from what is typically a spherical form lacking any obvious local field structure into some alternate geometry that can provide appropriate distinguishable local field profiles.

Depending on size, the agents' spectral components are detected either directly through chemical shift imaging, or indirectly through a magnetization transfer imaging protocol similar to those used with CEST agents. A difference with these engineered agents, however, is that the magnetization is transferred not via a chemical exchange between a bound and a free proton, but via self-diffusion of water into and out of the engineered cavity field region. The exchange rate is therefore not chemically determined; it depends on structure geometry, and, more significantly, on structure size. Fortuitously, because diffusion time periods scale with the square of distance, higher exchange rates, which allow for greater detection sensitivity, result from smaller, less biologically invasive, structures. Specifically, for any given quantity of precursor material, the nature of the diffusion driven exchange process means that it is often better to divide that material into a larger number of smaller structures than into a smaller number of larger ones. Higher exchange rates might lead to unfavorable broadening of the structure's resonance linewidth, but given the large resonance shifts possible, this should become a limiting problem only once structures shrink to below approximately 100 nm. This means that artificial engineered agents can be more sensitive, and used in lower concentrations, than more natural chemical exchange based agents [40].

NIH-PA Author Manuscript

NIH-PA Author Manuscript

NIH-PA Author Manuscript

Beyond the move from contrast to “color”, these engineered resonance shifters also offer the potential of MRI sensing of physiological conditions. Such sensing may take the form of a conditional, discrete turning on or off of the resonance shifting capabilities by enabling or blocking access to the inner, homogeneous field region (for an example, see Fig. 6), or by designing agents that simply fall apart under appropriate conditions. One can easily imagine numerous possibilities for making the agents functional, for example, blocking or supporting materials that might melt when a certain temperature is exceeded or that might be designed to disintegrate in the presence of some particular cleaving enzyme. Note that whether the spectral signal is present or not, the ability to image an agent's spatial position, which depends on the T_2^* signal, is unaffected. Thus it is possible to distinguish whether the disappearance of the shifted spectral signal is indeed due to some local condition that is being sensed or is simply the case of a missing resonance shifting agent.

The agents also offer the prospect of continuous, quantitative sensing. With resonance shifts determined by agent geometry, resonance shifters that are engineered to have shapes that can dynamically vary in response to surrounding conditions, could provide real-time readout of local physiological variables such as pH, temperature, analyte concentrations, and so forth. At the time of writing such agents with dynamically variable resonances are still in early stages of development, but, with the possibility to engineer directly their sensitivity and dynamic range, the potential as a sensor platform seems interesting.

Unlike other MRI agents, which are chemically synthesized, thus far these engineered multispectral agents have all been microfabricated [57]. Whether or not the advantages of such engineered structures are sufficient to outweigh their more complex (and costly) microfabrication procedures remains an open question. It should be noted, however, that there is nothing fundamental precluding these agents from also being chemically synthesized, or perhaps more likely, from being produced via some combination of bottom-up and top-down technologies. At present it is unclear whether a purely chemical synthesis approach could provide as great a degree of agent monodispersity as can a top-down microfabrication approach; but even with the broadened linewidths and the concomitant signal loss that comes with reduced monodispersity, the enhanced functionality may still render such engineered agents of value.

These geometrical resonance shifts are the first microfabricated MRI contrast agents. Continually improving microfabrication equipment and the burgeoning research fields of bottom-up nanotechnology and nanobiotechnology, mean that both the tools and the experience to fabricate or synthesize novel micro- and nanostructures are becoming ever better and more commonplace. Current microengineered MRI resonant shifting agent sizes already extend down below the single micron scale, small enough already to be endocytosed by many different cell types. There is likely a path to miniaturize the structures down to the 100 nm level. Given the array of accessible biology that such size ranges allow, and the increased functionality that such tailor made devices offer, it seems likely we will see ever more artificially engineered micro- and nanoscale sensors.

NIH-PA Author Manuscript

NIH-PA Author Manuscript

NIH-PA Author Manuscript

Conclusion

The wireless amplified detector and the fabricated contrast agents represent two recent approaches towards engineering increased capabilities in MRI. The wireless amplifier aims to increase the MRI sensitivity by parametrically amplifying the locally detected MR signals. The micro-engineered particles aims to enhance the specificity of contrast agents by adding a large frequency shift range with ferromagnetic materials in well-defined geometry. Benefiting from state-of-the-art micro-fabrication techniques and the further development of nonlinear RF sensing materials, the wireless amplifier can be further miniaturized, potentially down to the 100 μm scale level which will make it possible to implant MRI detectors for a wide range of applications. At this scale, the detector and the resonator may be integrated into a single device to enable novel sensing capabilities by MRI. The future use of the increasing sophistication of microfabrication and increasing range of novel nanomaterials leads to the conclusion that the future is exciting for microengineering novel MRI detectors and sensors.

Acknowledgments

This research was supported by the Intramural Research Program of the NIH, NINDS.

References

[1]. Olson DL, Peck TL, Webb AG, Magin RL, Sweedler JV. High-Resolution Microcoil H-1-Nmr for Mass-Limited, Nanoliter-Volume Samples. Science. 1995; 270:1967–1970.

[2]. Webb AG. Radiofrequency microcoils in magnetic resonance. Progress in Nuclear Magnetic Resonance Spectroscopy. 1997; 31:1–42.

[3]. Schnall MD, Barlow C, Subramanian VH, Leigh JS. Wireless Implanted Magnetic-Resonance Probes for in vivo NMR. Journal of Magnetic Resonance. 1986; 68:161–167.

[4]. Hollett MD, Cofer GP, Johnson GA. In situ magnetic resonance microscopy. Investigative Radiology. 1987; 22:965. [PubMed: 3440731]

[5]. Farmer THR, Johnson GA, Cofer GP, Maronpot RR, Dixon D, Hedlund LW. Implanted Coil Mr Microscopy of Renal Pathology. Magnetic Resonance in Medicine. 1989; 10:310–323. [PubMed: 2733588]

[6]. Morikawa S, Inubushi T, Kito K, Amano S. Long-Term Observation of in-Vivo P-31 Nmr-Spectra in Carbon Tetrachloride-Intoxicated Rabbit Liver Using Implanted Wireless Surface Coil. Nmr in Biomedicine. 1995; 8:3–8. [PubMed: 7547182]

[7]. Summers RM, Hedlund LW, Cofer GP, Gottsman MB, Manibo JF, Johnson GA. Mr Microscopy of the Rat Carotid-Artery after Balloon Injury by Using an Implanted Imaging Coil. Magnetic Resonance in Medicine. 1995; 33:785–789. [PubMed: 7651114]

[8]. Berry L, Renaud L, Kleimann P, Morin P, Armenean M, Saint-Jalmes H. Development of implantable detection microcoils for minimally invasive NMR spectroscopy. Sensors and Actuators a-Physical. 2001; 93:214–218.

[9]. Silver X, Ni WX, Mercer EV, Beck BL, Bossart EL, Inglis B, Mareci TH. In vivo H-1 magnetic resonance imaging and spectroscopy of the rat spinal cord using an inductively-coupled chronically implanted RF coil. Magnetic Resonance in Medicine. 2001; 46:1216–1222. [PubMed: 11746589]

[10]. Bilgen M, Elshafiey I, Narayana PA. In vivo magnetic resonance microscopy of rat spinal cord at 7 T using implantable RF coils. Magnetic Resonance in Medicine. 2001; 46:1250–1253. [PubMed: 11746595]

[11]. Quick HH, Kuehl H, Kaiser G, Bosk S, Debatin JF, Ladd ME. Inductively coupled stent antennas in MRI. Magnetic Resonance in Medicine. 2002; 48:781–790. [PubMed: 12417992]

NIH-PA Author Manuscript

NIH-PA Author Manuscript

NIH-PA Author Manuscript

[12]. Bilgen M. Magnetic resonance microscopy of spinal cord injury in mouse using a miniaturized implantable RF coil. Journal of Neuroscience Methods. 2007; 159:93–97. [PubMed: 16890294]

[13]. Kadjo, A.; Baxan, N.; Briguet, A.; Graveron-Demilly, D.; Fakri-Bouchet, L.; Cespuglio, R.; Rousset, C. In vivo animal NMR studies using implantable micro coil, in: IST 2008 - IEEE Workshop on Imaging Systems and Techniques Proceedings; Chania, Crete. 2008. p. 294

[14]. Rivera DS, Cohen MS, Clark WG, Chu AC, Nunnally RL, Smith J, Mills D, Judy JW. An Implantable RF Solenoid for Magnetic Resonance Microscopy and Microspectroscopy. Ieee Transactions on Biomedical Engineering. 2012; 59:2118–2125. [PubMed: 22156945]

[15]. Ginefri JC, Rubin A, Tatoulian M, Woytasik M, Boumezbeur F, Djema B, Poirier-Quinot M, Lethimonnier F, Darrasse L, Dufour-Gergam E. Implanted, Inductively-Coupled, Radiofrequency Coils Fabricated On Flexible Polymeric Material: Application To In Vivo Rat Brain Mri At 7 T. Journal of Magnetic Resonance. 2012

[16]. Wirth ED, Mareci TH, Beck BL, Fitzsimmons JR, Reier PJ. A Comparison of an Inductively-Coupled Implanted Coil with Optimized Surface Coils for in-Vivo Nmr Imaging of the Spinal-Cord. Magnetic Resonance in Medicine. 1993; 30:626–633. [PubMed: 8259063]

[17]. Arnder LL, Shattuck MD, Black RD. Signal-to-noise ratio comparison between surface coils and implanted coils. Magnetic Resonance in Medicine. 1996; 35:727–733. [PubMed: 8722824]

[18]. Ciocan R, Lenkinski RE, Bernstein J, Bancu M, Marquis R, Ivanishev A, Kourtelidis F, Matsui A, Borenstein J, Frangioni JV. MRI Contrast Using Solid-State, B-1-Distorting, Microelectromechanical Systems (MEMS) Microresonant Devices (MRDs). Magnetic Resonance in Medicine. 2009; 61:860–866. [PubMed: 19189289]

[19]. Murphyboesch J, Koretsky AP. An In vivo NMR Probe Circuit for Improved Sensitivity. Journal of Magnetic Resonance. 1983; 54:526–532.

[20]. Atalar E, Bottomley PA, Ocali O, Correia LCL, Kelemen MD, Lima JAC, Zerhouni EA. High resolution intravascular MRI and MRS by using a catheter receiver coil. Magnetic Resonance in Medicine. 1996; 36:596–605. [PubMed: 8892213]

[21]. Wildermuth S, Zimmermann GG, Debatin JF. Vascular applications of interventional MRI. Radiology. 1998; 38:210–217.

[22]. Hillenbrand CM, Elgort DR, Wong EY, Reykowski A, Wacker FK, Lewin JS, Duerk JL. Active device tracking and high-resolution intravascular MRI using a novel catheter-based, opposed-solenoid phased array coil. Magnetic Resonance in Medicine. 2004; 51:668–675. [PubMed: 15065238]

[23]. Ladd, ME.; Quick, HH.; Boesiger, P.; Mckinnon, G. RF heating of actively visualized catheters and guidewires. Proceedings of the 17th Annual Meeting of ISMRM; 1998. p. 473

[24]. Konings MK, Bartels LW, Smits HFM, Bakker CJG. Heating around intravascular guidewires by resonating RF waves. Journal of Magnetic Resonance Imaging. 2000; 12:79–85. [PubMed: 10931567]

[25]. Park SM, Kamondetdacha R, Amjad A, Nyenhuis JA. MRI safety: RF-induced heating near straight wires. IEEE Transactions on Magnetics. 2005; 41:4197.

[26]. Wiltshire MCK, Pendry JB, Young IR, Larkman DJ, Gilderdale DJ, Hajnal JV. Microstructured magnetic materials for RF flux guides in magnetic resonance imaging. Science. 2001; 291:849–851. [PubMed: 11157159]

[27]. Weiss S, Vernickel P, Schaeffter T, Schulz V, Gleichl B. Transmission line for improved RF safety of interventional devices. Magnetic Resonance in Medicine. 2005; 54:182–189. [PubMed: 15968655]

[28]. Vernickel P, Schulz V, Weiss S, Gleich B. A safe transmission line for MRI. Ieee Transactions on Biomedical Engineering. 2005; 52:1094–1102. [PubMed: 15977738]

[29]. Fandrey S, Weiss S, Muller J. Development of an Active Intravascular MR Device With an Optical Transmission System. Ieee Transactions on Medical Imaging. 2008; 27:1723–1727. [PubMed: 19033088]

[30]. Fandrey S, Weiss S, Muller J. A novel active MR probe using a miniaturized optical link for a 1.5-T MRI scanner. Magnetic Resonance in Medicine. 2012; 67:148–155. [PubMed: 21837807]

[31]. Yak N, Anderson KJT, Wright GA. Tuning and amplification strategies for intravascular imaging coils. Magnetic Resonance in Medicine. 2011 In Press.

NIH-PA Author Manuscript

NIH-PA Author Manuscript

NIH-PA Author Manuscript

[32]. Hoult DI, Tomanek B. Use of mutually inductive coupling in probe design. Concepts in Magnetic Resonance (magnetic resonance engineering). 2002; 15:262–285.

[33]. Berke, HR. Solid State NMR Probe, U.S. Patent, 4,672,972 (issued Jun. 16, 1987).

[34]. Martius, S.; Heir, O.; Vester, M.; Biber, S.; Nistler, J. Wireless local coil signal transmission using a parametric upconverter. Proceedings of the 17th Annual Meeting of ISMRM; Honolulu, Hawaii, USA. 2009. p. 2934

[35]. Cork, P.; Hulbert, AP.; Hunt, J. Parametric Amplifier Device, U.S. Patent Application No. 12/753132, Publication No. 20100253349. (published Oct. 7, 2010)

[36]. Syms RRA, Floume T, Young IR, Solymar L, Rea M. Parametric Amplification of Magnetic Resonance Images. Ieee Sensors Journal. 2012; 12:1836–1845.

[37]. Qian C, Murphy-Boesch J, Dodd S, Koretsky A. Sensitivity enhancement of remotely coupled NMR detectors using wirelessly powered parametric amplification. Magnetic Resonance in Medicine. 2012; 68:989–996. [PubMed: 22246567]

[38]. Collin, RE. Foundations for Microwave Engineering. McGraw-Hill; NY: 1966.

[39]. Manley JM, Rowe HE. Some General Properties of Nonlinear Elements.1. General Energy Relations. Proceedings of the Institute of Radio Engineers. 1956; 44:904–913.

[40]. Zabow G, Dodd S, Moreland J, Koretsky A. Micro-engineered local field control for high-sensitivity multispectral MRI. Nature. 2008; 453:1058–1052. [PubMed: 18563157]

[41]. Zabow G, Koretsky AP, Moreland J. Design and fabrication of a micromachined multispectral magnetic resonance imaging agent. Journal of Micromechanics and Microengineering. 2009; 19

[42]. Zabow G, Dodd SJ, Moreland J, Koretsky AP. The fabrication of uniform cylindrical nanoshells and their use as spectrally tunable MRI contrast agents. Nanotechnology. 2009; 20

[43]. Chikazumi, S. Physics of Ferromagnetism. Oxford University Press; NY: 1997.

[44]. Chan WCW, Nie SM. Quantum dot bioconjugates for ultrasensitive nonisotopic detection. Science. 1998; 281:2016–2018. [PubMed: 9748158]

[45]. Bruchez M, Moronne M, Gin P, Weiss S, Alivisatos AP. Semiconductor nanocrystals as fluorescent biological labels. Science. 1998; 281:2013–2016. [PubMed: 9748157]

[46]. Alivisatos P. The use of nanocrystals in biological detection. Nature Biotechnology. 2004; 22:47–52.

[47]. Anker JN, Hall WP, Lyandres O, Shah NC, Zhao J, Van Duyne RP. Biosensing with plasmonic nanosensors. Nature Materials. 2008; 7:442–453.

[48]. Mason, WT. Fluorescent and Luminescent Probes for Biological Activity. Academic Press; London: 1999.

[49]. Ward KM, Aletras AH, Balaban RS. A new class of contrast agents for MRI based on proton chemical exchange dependent saturation transfer (CEST). Journal of Magnetic Resonance. 2000; 143:79–87. [PubMed: 10698648]

[50]. Zhang SR, Merritt M, Woessner DE, Lenkinski RE, Sherry AD. PARACEST agents: Modulating MRI contrast via water proton exchange. Accounts of Chemical Research. 2003; 36:783–790. [PubMed: 14567712]

[51]. Woods M, Donald EWC, Sherry AD. Paramagnetic lanthanide complexes as PARACEST agents for medical imaging. Chemical Society Reviews. 2006; 35:500–511. [PubMed: 16729144]

[52]. Aime S, Castelli DD, Terreno E. Highly sensitive MRI chemical exchange saturation transfer agents using liposomes. Angewandte Chemie-International Edition. 2005; 44:5513–5515.

[53]. Bulte JWM, Kraitchman DL. Iron oxide MR contrast agents for molecular and cellular imaging. Nmr in Biomedicine. 2004; 17:484–499. [PubMed: 15526347]

[54]. Jung CW, Jacobs P. Physical and Chemical-Properties of Superparamagnetic Iron-Oxide Mr Contrast Agents - Ferumoxides, Ferumoxtran, Ferumoxsil. Magnetic Resonance Imaging. 1995; 13:661–674. [PubMed: 8569441]

[55]. Wang YXJ, Hussain SM, Krestin GP. Superparamagnetic iron oxide contrast agents: physicochemical characteristics and applications in MR imaging. European Radiology. 2001; 11:2319–2331. [PubMed: 11702180]

[56]. Shapiro EM, Skrtic S, Koretsky AP. Sizing it up: Cellular MRI using micron-sized iron oxide particles. Magnetic Resonance in Medicine. 2005; 53:329–338. [PubMed: 15678543]

[57]. Madou, MJ. Fundamentals of Microfabrication: the Science of Miniaturization. CRC Press; Florida: 2002.

NIH-PA Author Manuscript

NIH-PA Author Manuscript

NIH-PA Author Manuscript

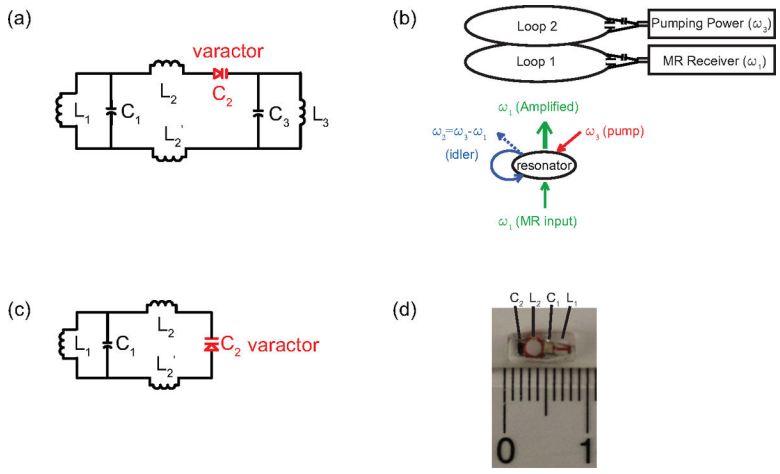

Fig. 1.

(a) A parametric triple frequency resonator with one capacitor C_2 substituted by a varactor diode. (b) The schematic illustration of parametric amplification process. (c) A parametric double frequency resonator as a simplified circuit design. (d) An enlarged photograph of a double frequency parametric resonator encapsulated by Polydimethylsiloxane (PDMS).

NIH-PA Author Manuscript NIH-PA Author Manuscript NIH-PA Author Manuscript

NIH-PA Author Manuscript

NIH-PA Author Manuscript

NIH-PA Author Manuscript

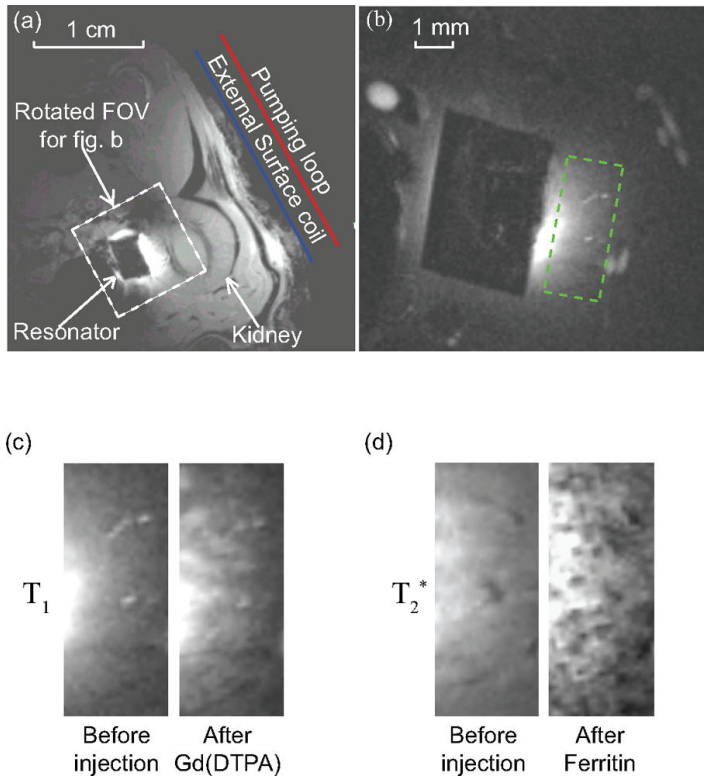

Fig. 2.

Axial images of a rat kidney obtained by Gradient Refocused Echo sequence. (a) A low resolution image acquired without parametric amplification to locate the position of the parametric resonator, with the following acquisition parameters: TE = 6 ms, TR = 357 ms, FA = 30 deg, NS = 1, in-plane resolution 156 × 156 μm^2, FOV = 4 × 4 cm^2, slice thickness = 1 mm. (b) A representative example of high resolution image acquired in the presence of parametric amplification, with a FOV defined by the white dashed box (a). The readout direction for image acquisition is aligned approximately perpendicular to the external pick up loop to filter out the intense surface signal. The acquisition parameters for high resolution T_1-weighted images are: TE = 3.6 ms, TR = 37.4 ms, FA = 40 deg, in-plane resolution = 70 × 70 μm^2, FOV = 9 × 9 mm^2, slice thickness = 0.2 mm, NEX = 40 (experiment time = 3.2 mins). The acquisition parameters for T_2*-weighted images are: TE = 10 ms, TR = 58 ms, FA = 20 deg, experiment time = 5.8 mins, with other parameters remaining the same as T_1-weighted images. The black rectangular region in the center of (b) is the PDMS coated resonator. the region of interest defined by the green dashed box. (c) High resolution T_1-weighted image before and after the injection of a bolus Gd(DTPA) of 5 μmol/kg of body weight, showing the region of interest defined by the green dashed box in (b). (d) High resolution T_2*-weighted image before and after the injection of a bolus cationized ferritin of 113 mg/kg of body weight.

NIH-PA Author Manuscript
NIH-PA Author Manuscript
NIH-PA Author Manuscript

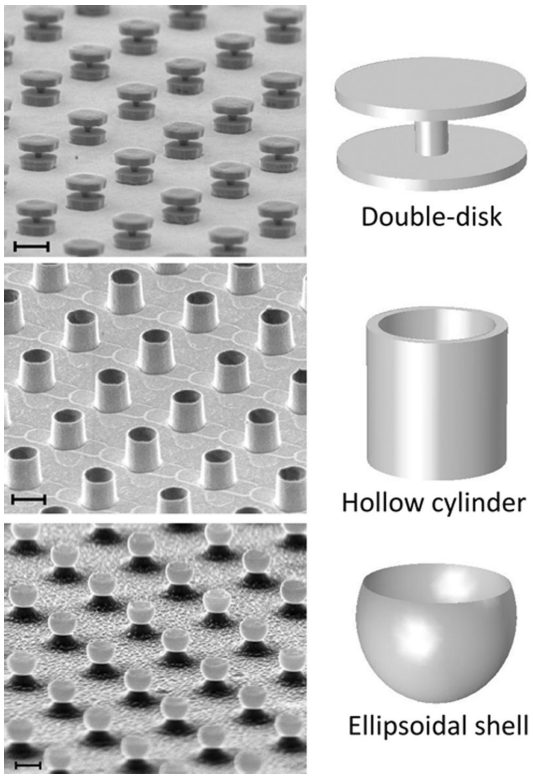

Fig. 3.

Angled scanning electron micrographs (SEM) of microfabricated resonance shifting MRI agents in the form of (top to bottom): spaced double-disk pairs, hollow cylinders, and ellipsoidal shells. Scale bars (top to bottom): 10 μm, 2 μm, and 2 μm. Idealized shape schematics shown alongside.

NIH-PA Author Manuscript

NIH-PA Author Manuscript

NIH-PA Author Manuscript

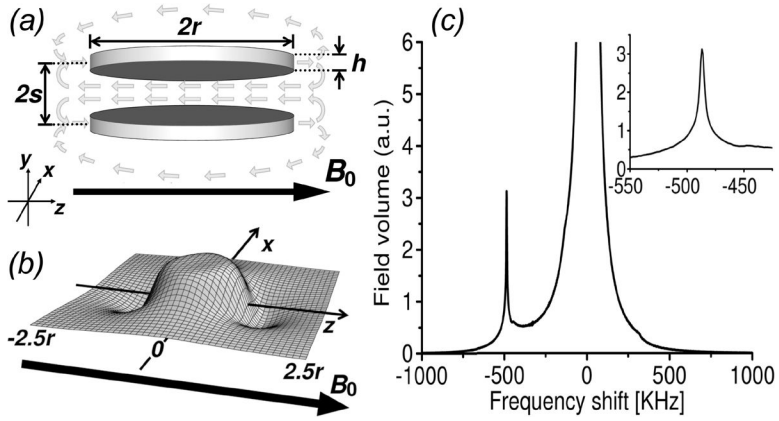

Fig. 4.

Resonance shifting agent structure and fields: (*a*) schematic of double-disk design (for clarity, non-magnetic spacer elements not shown) showing magnetizing B_0 field (dark arrow) and resulting structure field (light arrows), (*b*) sample numerical calculation of the (negative) field magnitude profile in the horizontal mid-plane passing through a double-disk structure, showing uniformly shifted field magnitude between the disks, (*c*) sample histogram recording the magnetic field magnitudes (or equivalently, Larmor precession frequencies) surrounding a double-disk structure that shows the background water signal and the shifted spectral peak due to the double-disk structure; inset shows a blow-up around the shifted peak region. Calculations are for structures with disk radii r = 1 μm, center-to-center disk spacings 2s = 0.85 μm, and disk thickness h = 50 nm. They are assumed made from nickel with saturation magnetic polarization density of 0.6 T. (Reproduced with permission from Zabow et al., J. Micromech. Microeng. 2009)

NIH-PA Author Manuscript
NIH-PA Author Manuscript
NIH-PA Author Manuscript

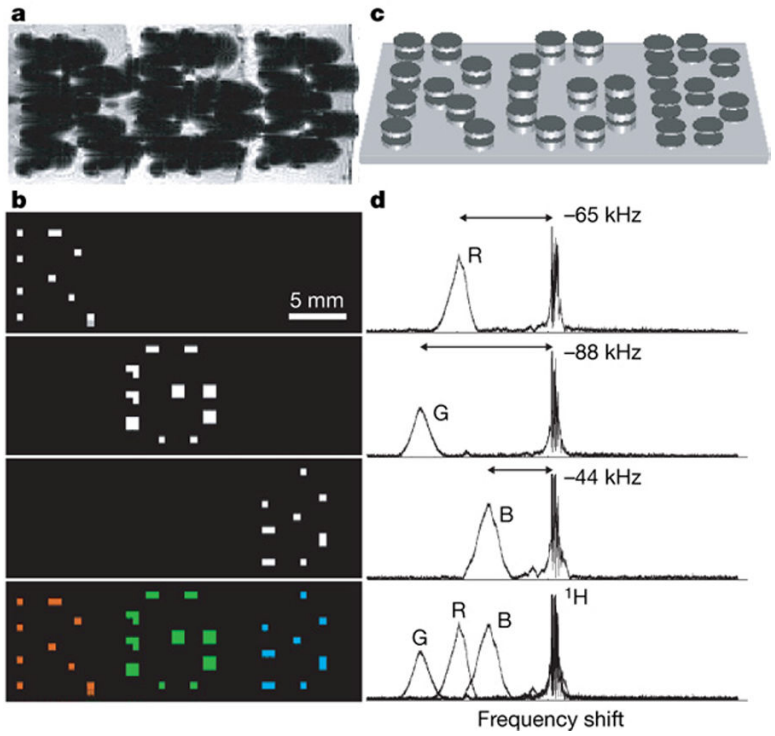

Fig. 5.

Multi-spectral MRI. a – d, Chemical shift imaging of demonstration 1.25-mm-diameter particles magnetized by B0. Particle frequency was varied by changing the thickness of electroplated nickel layers that formed the magnetizable disk pairs. As with normal SPIO detection, magnetic dephasing due to the particles' external fields enables the spatial imaging shown in the gradient-echo MRI (a). However, comparison between a and the chemical shift images (b) shows that the additional spectral information both differentiates between particle types and improves particle localization. The particles are shown schematically (not to scale) in c. With particle spectra (d, to the right of the corresponding chemical shift images in b) shifted well clear of the water proton line, different planes in the chemical shift imaging map isolate different particle types for unambiguous color coding with minimal background interference (b, bottom panel). Although still visible in the gradient-echo image, the top corner particle of the letter `B' was damaged, causing its shifted frequency peak to vanish. (Reproduced with permission from Zabow et al.,Nature 2008)

NIH-PA Author Manuscript
NIH-PA Author Manuscript
NIH-PA Author Manuscript

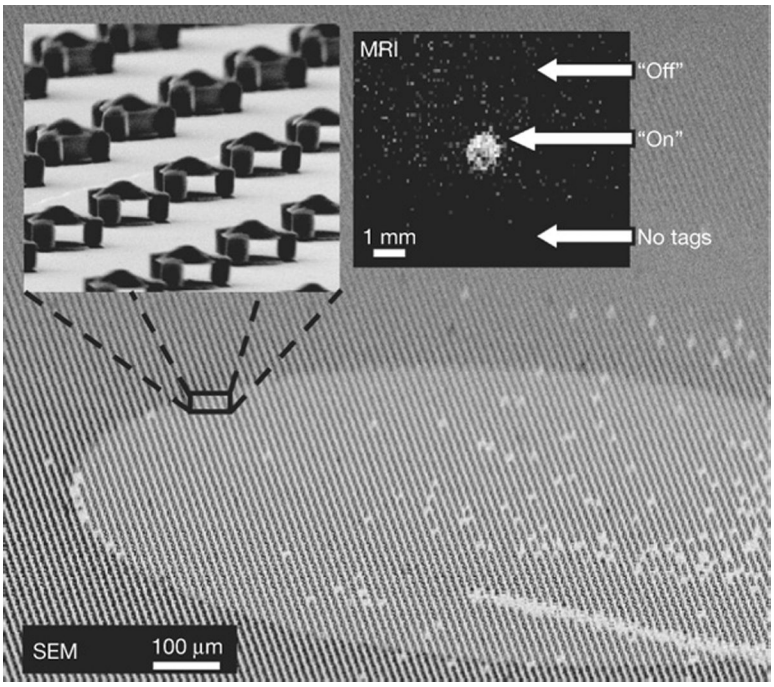

Fig. 6.

Controlling diffusion to turn tags on or off. Main panel, high tilt-angle SEM image showing a square array of R = 2.5 µm particles. Except for a defined circular region, all particles have their interiors filled, blocking water diffusion. Top left inset, a higher magnification SEM image of the boundary between open and filled particles. Top right inset, the resulting background-subtracted chemical shift MRI showing transferred magnetization saturation from the particles' shifted resonance. Signal is visible from those particles that have water diffusing through their open interior region (labelled 'On') but not from those particles that have their interiors filled (labelled 'Off'). The bottom of the image shows a region that contains no particles (labelled 'No tags'), providing a null background signal comparison. A scratch (seen at the lower right corner) removed ~100 particles (about 10–20 per voxel). Its visibility in the MR image suggests the potential for high-resolution imaging to spectrally distinguish individual such particles. (Reproduced with permission from Zabow et al., Nature 2008)